High Power Laser Science and Engineering, (2024), Vol. 12, e38, 8 pages.
doi:10.1017/hpl.2024.21

HIGH POWER LASER SCIENCE AND ENGINEERING

RESEARCH ARTICLE

Design and optimization methods towards a 10 kW high beam quality fiber laser based on the counter tandem pumping scheme

Ruixian Li[1], Hanshuo Wu[1,2,3], Hu Xiao[1,2,3], Zilun Chen[1,2,3], Jinyong Leng[1,2,3], Liangjin Huang[1,2,3], Zhiyong Pan[1,2,3], and Pu Zhou[1]

[1] *College of Advanced Interdisciplinary Studies, National University of Defense Technology, Changsha, China*

[2] *Nanhu Laser Laboratory, National University of Defense Technology, Changsha, China*

[3] *Hunan Provincial Key Laboratory of High Energy Laser Technology, Changsha, China*

(Received 27 January 2024; revised 7 March 2024; accepted 17 April 2024)

Abstract

In this study, we investigated the influence of fiber parameters on stimulated Raman scattering (SRS) and identified a unique pattern of SRS evolution in the counter tandem pumping configuration. Our findings revealed that the SRS threshold in counter-pumping is predominantly determined by the length of the output delivery fiber rather than the gain fiber. By employing the counter tandem pumping scheme and optimizing the fiber parameters, a 10 kW fiber laser was achieved with beam quality M^2 of 1.92. No mode instability or severe SRS limitation was observed. To our knowledge, this study achieved the highest beam quality in over 10 kW fiber lasers based on conventional double-clad Yb-doped fiber.

Keywords: fiber laser; high beam quality; high power; stimulated Raman scattering; tandem pumping

1. Introduction

Tandem pumping is a technique that uses fiber lasers as pump sources instead of laser diodes. It has been proposed and demonstrated as a robust pathway to achieve high-power high-brightness Yb-doped fiber lasers (YDFLs)[1–4]. One of the key challenges for power scaling of tandem pumping is stimulated Raman scattering (SRS)[5]. The low absorption cross-section of Yb ions at the tandem pumping wavelength (e.g., 1018 nm) requires long gain fiber for adequate pump absorption, resulting in a relatively low SRS threshold. In addition, recent studies have shown that SRS might trigger quasi-static mode distortion[6–8] or dynamic mode instability (MI)[9–13], which could degrade the beam quality and directivity of the fiber laser systems. Therefore, mitigating SRS effect is crucial for tandem pumping towards higher power with good beam quality.

To overcome SRS limitations, many effective approaches have been proposed[14–20]. For tandem-pumped YDFLs, one common and practical method is to enlarge the fiber core, as the Raman Stokes gain is inversely proportional to the fiber core area. This method has enabled the experimental demonstration of 10 kW level tandem-pumped fiber amplifiers with an ultra-large core (>44 μm) YDF[21–24]. However, the beam quality was not good due to the lack of mode control means in such large cores. Some functional specialty fibers achieved good balance in SRS and mode control[25–29], but they are not widely used in high-power fiber laser systems due to their complex fabrication process, high cost and incompatibility with commercial fibers[30].

For a given fiber, counter-pumping has a higher SRS threshold compared to co-pumping[31,32]. In 2009, IPG Photonics developed a 10 kW single-mode fiber laser based on counter tandem pumping, as suggested in Ref. [33]. However, technical details such as the YDF parameters and pump coupling methods have not yet been comprehensively disclosed. In our previous study, we have demonstrated an 8.38 kW counter tandem-pumped fiber amplifier based on conventional double-clad YDF[34]. For such a high-power laser, the distribution of Raman Stokes gain along the fiber in counter-pumping is significantly distinct from that in co-pumping, thus potentially necessitating a differentiated

Correspondence to: Hu Xiao and Pu Zhou, College of Advanced Interdisciplinary Studies, National University of Defense Technology, Changsha 410073, China. Email: xhwise@163.com (H. Xiao); zhoupu203@163.com (P. Zhou)

approach for SRS suppression. To our knowledge, there is a lack of detailed research on SRS evolution in counter tandem pumping.

In this paper, we present our continued efforts to enhance the SRS threshold by optimizing fiber parameters. Based on the steady-state rate equation, we analyzed the influence of fiber length on the SRS threshold in co/counter-pumping schemes. Our findings reveal that the length of the delivery fiber (DF) exerts a more significant influence on SRS compared to the YDF. To maintain the advantages of counter-pumping, a marginally longer YDF is acceptable to ensure adequate pump absorption. Nevertheless, the DF length should be minimized for SRS suppression. Through optimizing the fiber, we achieved 10 kW output power with $M^2 = 1.92$ based on conventional 30/250 μm double-clad YDF.

2. SRS suppression analysis

We aim to generate over 10 kW of power employing conventional double-clad fiber. At this level of power, the SRS used to be the main limitation for power scaling. In this section, to develop guidelines for the fiber optimization, the impact of YDF and output DF on the SRS threshold is theoretically and experimentally investigated.

2.1. Rate equations

To simulate the power evolution in tandem-pumped amplifiers, we built a theoretical model based on steady-state rate equations that take into account SRS[35]. In YDF, the power evolution of the laser satisfies the following equations:

$$\frac{N_2(z)}{N} = \left\{ \frac{\left[P_p^+(z)+P_p^-(z)\right]\sigma_{ap}\lambda_p\Gamma_p}{hcA_c} + \frac{\left[P_s^+(z)+P_s^-(z)\right]\sigma_{as}\lambda_s\Gamma_s}{hcA_c} + \frac{\left[P_R^+(z)+P_R^-(z)\right]\sigma_{aR}\lambda_R\Gamma_R}{hcA_c} \right\} \left\{ \frac{1}{\tau} + \frac{\left[P_p^+(z)+P_p^-(z)\right](\sigma_{ap}+\sigma_{ep})\lambda_p\Gamma_p}{hcA_c} + \frac{\left[P_s^+(z)+P_s^-(z)\right](\sigma_{es}+\sigma_{as})\lambda_s\Gamma_s}{hcA_c} + \frac{\left[P_R^+(z)+P_R^-(z)\right](\sigma_{Rs}+\sigma_{Rs})\lambda_R\Gamma_R}{hcA_c} \right\}^{-1}. \tag{1}$$

$$\pm\frac{dP_p^{\pm}(z)}{dz} = -\Gamma_p\left\{\sigma_a(\lambda_p)N - \left[\sigma_a(\lambda_p)+\sigma_e(\lambda_p)\right]N_2(z)\right\} \times P_p^{\pm}(z) - \alpha(\lambda_p)P_p^{\pm}(z), \tag{2}$$

$$\pm\frac{dP_s^{\pm}(z)}{dz} = \Gamma_s\{[\sigma_e(\lambda_s)+\sigma_a(\lambda_s)]N_2(z) - \sigma_a(\lambda_s)N\}P_s^{\pm}(z) + \Gamma_s\sigma_e(\lambda_s)N_2(z)P_0 - \frac{g_R}{A_{eff}^s}\frac{\lambda_R}{\lambda_s}\left[P_R^+(z)+P_R^-(z)\right] \times P_s^{\pm}(z) - \alpha(\lambda_s)P_s^{\pm}(z), \tag{3}$$

$$\pm\frac{dP_R^{\pm}(z)}{dz} = \Gamma_R\{[\sigma_e(\lambda_R)+\sigma_a(\lambda_R)]N_2(z) - \sigma_a(\lambda_R)N\}P_R^{\pm}(z) + \Gamma_R\sigma_e(\lambda_R)N_2(z)P_0 + \frac{g_R}{A_{eff}^R}\left[P_s^+(z)+P_s^-(z)\right] \times P_R^{\pm}(z) - \alpha(\lambda_R)P_R^{\pm}(z). \tag{4}$$

In Equations (1)–(4), P represents power. The subscripts p, s and R correspond to the pump light, signal light and first-order Raman Stokes light at the wavelengths of λ_p, λ_s and λ_R, respectively. The superscripts + and – represent the forward-propagating and backward-propagating lasers; N is the total dopant concentration of Yb ions; $N_2(z)$ is the upper-level densities at the fiber position z; σ_a and σ_e are the absorption and emission cross-sections of Yb ions; Γ is the mode field overlapping factor to the core area A_c; A_{eff} is the mode field area; τ is the spontaneous lifetime of the upper laser level; C is the light velocity in vacuum; H is the Planck constant; G_R is the Raman gain coefficient of the fiber; and α is the loss coefficient of the fiber. In Equations (3) and (4), the first term is linked to Yb gain, the second term is related to spontaneous emissions of Yb ions, the third one corresponds to Raman gain and the last term is attributed to fiber loss.

In the output DF, the Yb ion does not play a role in the energy conversion process. Only the Raman gain converts the signal light to Raman Stokes light. As a result, the power coupling equations in DF are given by

$$\frac{dP_s^{\pm}(z)}{dz} = -\frac{g_R}{A_c}\frac{\lambda_R}{\lambda_s}\left[P_R^+(z)+P_R^-(z)\right]P_R^{\pm}(z) - \alpha(\lambda_s)P_s^{\pm}(z), \tag{5}$$

$$\frac{dP_R^{\pm}(z)}{dz} = \frac{g_R}{A_c}\left[P_s^+(z)+P_s^-(z)\right]P_R^{\pm}(z) - \alpha(\lambda_R)P_R^{\pm}(z). \tag{6}$$

To describe the total gain achieved by Raman Stokes light, which considers both Yb gain and Raman gain, we define SRS gain as follows:

$$G_{SRS}(z) = \begin{cases} \Gamma_R\{[\sigma_e(\lambda_R)+\sigma_a(\lambda_R)]N_2(z) - \sigma_a(\lambda_R)N\} \\ +\frac{g_R}{A_c}\left[P_s^+(z)+P_s^-(z)\right], \text{ in YDF,} \\ \frac{g_R}{A_c}\left[P_s^+(z)+P_s^-(z)\right], \text{ in DF.} \end{cases} \tag{7}$$

To simplify the analysis, we consider the signal, pump and Raman Stokes lasers as monochromatic light. This assumption is reasonable as the Raman gain remains nearly constant over a wide bandwidth of up to several THz[36]. Moreover, we assume that the signal and Raman Stokes lasers are single mode. Mode-related effects, such as mode competition, mode interference and mode coupling, are ignored in the simulation.

https://doi.org/10.1017/hpl.2024.21 Published online by Cambridge University Press

2.2. Numerical simulations

The relevant simulation parameters are listed in Table 1. Considering the accuracy of the SRS threshold calculations and to minimize the influence of high-order modes on SRS, we used relatively thin fibers with a core/cladding diameter of 25/250 μm with numerical aperture (NA) of 0.065. In this fiber, single-mode operation can be achieved by properly bending the YDF. To lower the SRS threshold for easy experimental verification, we used a long length of fiber comprising a 50 m YDF followed by a 10 m DF. The Raman gain is assumed to be constant and is taken from Ref. [35]. The absorption/emission cross-sections employed come from the measured data of our homemade YDF.

To explore the different SRS characteristics in co/counter-pumping, we examine the evolution of signal power, Raman Stokes power and SRS gain along the fiber in co-pumping (Figure 1(a)) and counter-pumping scheme (Figure 1(b)). The seed power and pump power are set as 100 and 3000 W, respectively. The initial Raman Stokes light at 1135 nm originates from spontaneous emissions of Yb ions, with a calculated power of 1.6×10^{-8} W. As shown in Figure 1, the signal power (red solid line) in both pumping schemes increases rapidly in the first 50 m of YDF and decreases in the last 10 m of DF. The SRS gain curves (green dotted line) are nearly proportional to the signal light intensity. The decline in gain noticed at the start of the YDF in co-pumping (Figure 1(a)) is mainly attributed to the decrease in Yb gain (the first term on the left of Equation (7)) at low power. In addition, the abrupt decrease in SRS gain at the beginning of DF is caused by the absence of Yb gain.

The main difference between the two schemes is that co-pumping shows a higher average SRS gain along the YDF. For the co-pumping situation, the Raman Stokes power (blue dashed line) increases from 1.6×10^{-8} to 16.2 W over a distance of 50 m YDF, and ultimately reaches 1086 W after passing through 10 m DF, corresponding to an average SRS gain of 1.8 and 1.83 dB/m in the YDF and DF, respectively. In the case of counter-pumping, the Raman Stokes power increases slowly in the YDF, from 1.6×10^{-8} to 5.41×10^{-4} W, corresponding to a gain of 0.91 dB/m, which is almost half the gain achieved in co-pumping. Then it increases to 0.1 W at the end of the DF, with an average SRS gain of 2.3 dB/m. The higher average gain in the DF indicates that the SRS threshold is more affected by DF. To be noted, in comparison to co-pumping, counter-pumping exhibits a more significant disparity in the average SRS gain between YDF and DF, which implies that the SRS threshold is more sensitive to variations in DF length in the counter-pumped amplifier.

Table 1. Main parameters in the simulation.

Parameter	Value	Parameter	Value
d_{core}	25 μm	g_R	0.98×10^{-13} m/W
d_{clad}	250 μm	N	6.8×10^{25} m^{-3}
NA_{core}	0.065	σ_a^{1018}	9.44×10^{-26} m^{-2}
L_{YDF}	50 m	σ_e^{1018}	7.3×10^{-25} m^{-2}
L_{DF}	10 m	σ_a^{1080}	2.29×10^{-27} m^{-2}
λ_p	1018 nm	σ_e^{1080}	2.82×10^{-25} m^{-2}
λ_s	1080 nm	σ_a^{1135}	1.16×10^{-28} m^{-2}
λ_R	1135 nm	σ_e^{1135}	6.46×10^{-26} m^{-2}

2.3. Experimental verification

To verify the accuracy of the simulation, we carried out a comparative experiment to study the impact of fiber length on the SRS. Figure 2 shows the experimental setup. The seed laser is a single-mode laser oscillator, which could produce 100 W level power at a wavelength of 1080 nm. The seed laser is injected into the amplifier through a mode field adaptor (MFA), a cladding light stripper (CLS 1) and a forward pump and signal combiner (FPSC). The gain fiber is a 50 m long 25/250 μm double-clad YDF with a core/inner-clad NA of 0.065/0.46 and an absorption coefficient of 0.28 dB/m at 1018 nm. The doping concentration and absorption/emission cross-sections are in line with Table 1. The 1018 nm pump lasers are launched into the amplifier through the FPSC

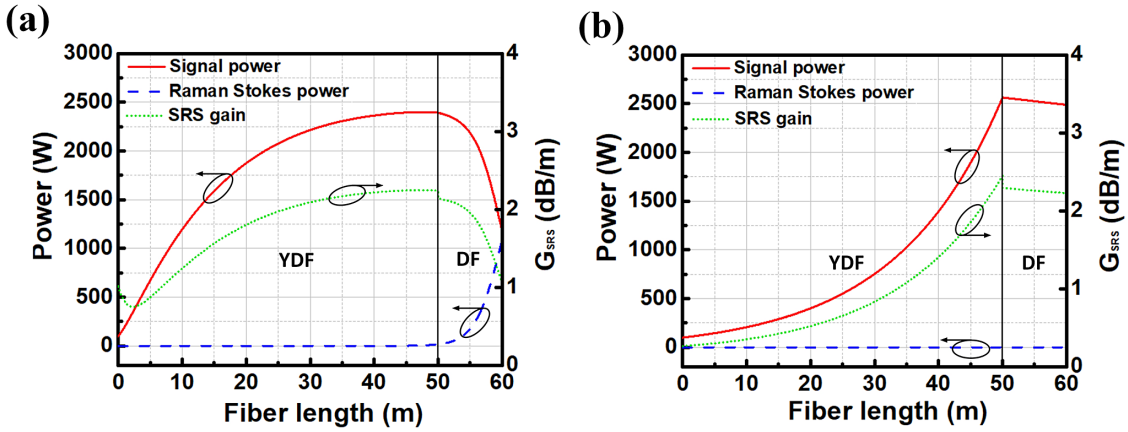

Figure 1. Evolution of signal power, Raman Stokes power and SRS gain along the fiber in (a) co-pumping and (b) counter-pumping schemes.

https://doi.org/10.1017/hpl.2024.21 Published online by Cambridge University Press

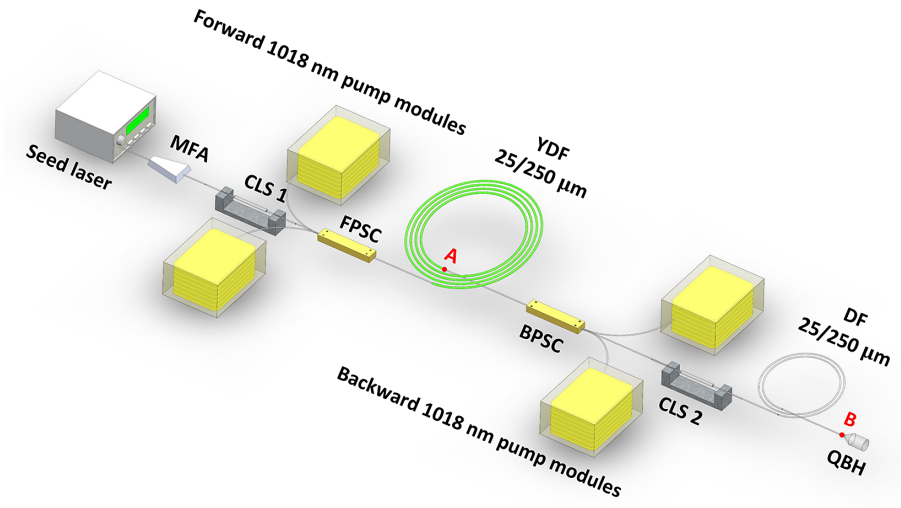

Figure 2. Experimental setup for investigating the impact of fiber length on the SRS threshold in co-pumping and counter-pumping amplifiers.

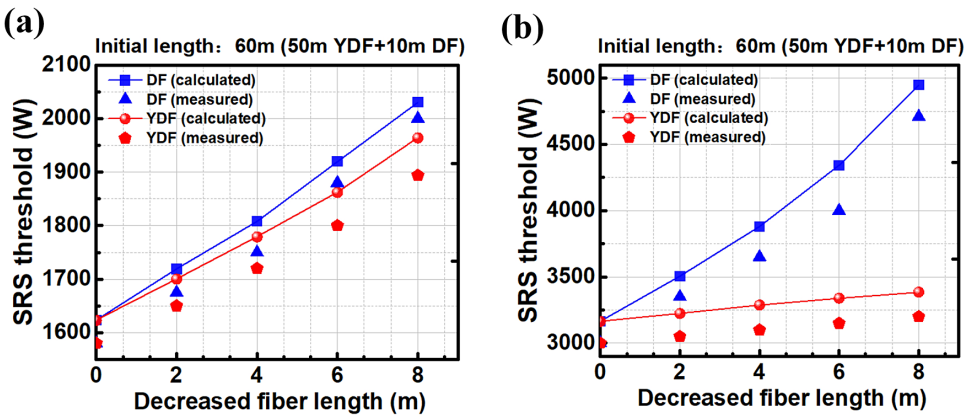

Figure 3. Experimentally measured and calculated SRS threshold versus the decreased length of DF (blue) and YDF (red) in (a) co-pumping and (b) counter-pumping schemes.

and backward pump and signal combiner (BPSC) for co-pumping and counter-pumping, respectively. A CLS 2 is employed after the BPSC to dump the unwanted cladding light. The laser is output from the quartz block holder (QBH). The DF from point A to point B has a core/inner-cladding diameter of 25/250 μm (NA = 0.065/0.46), with a total length of 10 m. By truncating the lengths of YDF and DF, the corresponding SRS threshold could be tested.

Figure 3 shows the experimentally measured and calculated SRS threshold variations as the fiber length decreases in the co-pumping and counter-pumping schemes. The SRS threshold is defined as the output power when the Raman-to-signal ratio reaches –30 dB[37]. The experimental and simulated results were in good agreement. In the co-pumping scheme (see Figure 3(a)), reducing the YDF and DF lengths by 8 m individually resulted in 314 and 420 W increase in the measured SRS threshold, respectively. This indicated that shortening either the DF or YDF length is an effective method for SRS suppression in co-pumping. However, in counter-pumping (refer to Figure 3(b)), shortening the YDF length was found to be less effective. Cutting off 8 m of YDF only led to a 200 W increase of the measured SRS threshold. In stark contrast, a decrease of 8 m in DF length caused an increase of up to 1710 W of the measured SRS threshold, which was 8.6 times greater than that of the truncated YDF of the same length. This finding suggested that counter-pumping allows for a relatively long YDF, leading to improved pump absorption without significantly decreasing the SRS threshold. Meanwhile, the length of the output DF should be carefully limited to suppress SRS.

3. The 10 kW fiber laser design and performance

3.1. Fiber selection

According to the calculation, it appears that achieving 10 kW output using the current 25/250 μm fiber would be quite challenging due to limitations of SRS. In our previous study, we experimentally demonstrated that the 30/250 μm YDF is able to generate an output power 8.38 kW without

https://doi.org/10.1017/hpl.2024.21 Published online by Cambridge University Press

indication of MI or SRS[34]. Figure 4 shows the calculated SRS threshold of the counter tandem-pumped amplifier versus the length of the 30/250 μm YDF. It is shown that the SRS threshold is expected to be over 10 kW by shortening the fiber length. However, the too short length of YDF would reduce the pump absorption, resulting in low laser efficiency. Considering the SRS threshold and pump absorption, the length of 30/250 μm YDF is selected to be approximately 38 m.

3.2. Experimental setup

Figure 5 shows the experimental setup of the 10 kW fiber laser system, which consists of a monolithic laser oscillator as a seed laser, a counter tandem-pumped amplifier and an optical measuring system. The seed laser emits 100 W continuous-wave lasers at a wavelength of approximately 1080 nm. The seed fiber pigtail has a core/cladding diameter of 15/130 μm, with a core NA of 0.08. To mitigate SRS, a chirped and tilted fiber Bragg grating (CTFBG) is integrated after the seed, which is made in-house with 15 dB Raman attenuation from 1131 to 1137 nm. The insertion loss of the CTFBG at 1080 nm is measured to be about 0.4 dB.

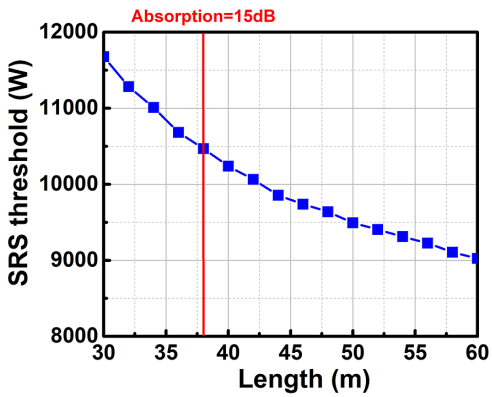

Figure 4. SRS threshold of 30/250 μm counter tandem-pumped amplifier versus YDF length. The DF length is set as 2 m in the calculation.

A homemade MFA is employed to reduce the beam quality degradation caused by the mismatch splicing of fibers. A CLS 1 is inserted before the amplifier stage to dump the residual pump laser for seed laser protection.

For the amplifier stage, a homemade 38 m long double-clad YDF is used as the gain medium, which has a core diameter of 30 μm (NA = 0.06) and a cladding diameter of 250 μm (NA = 0.46). The cladding absorption coefficient for the 1018 nm pump laser is measured to be approximately 0.4 dB/m at low power. The pump sources are five groups of power-combining-based 1018 nm fiber laser modules, which could provide a total of approximately 12,500 W pump lasers. With a homemade (6 + 1) × 1 BPSC, the pump lasers are injected into the gain fiber. The core/inner-cladding diameter of the input/output signal fiber of the BPSC is 30/250 μm. The pump fibers of BPSC are 135/155 μm multimode fibers (NA = 0.22), which are matched to the DFs of the pump sources. The signal insertion loss of BPSC is less than 1%, and the pump coupling efficiency is more than 98%. Another CLS 2 with 30/250 μm fiber is inserted after the BPSC to remove the unwanted cladding signal laser. The laser is output from a 30/250 μm QBH. The initial length of the output DF from point A to point B is 6 m, and is optimized to 1.5 m in the end. All the fiber components are mounted on a water-cooled heat sink.

In the optical measuring system, a collimator (CO) is used for laser beam collimation. Then, a highly reflective mirror (HRM) with a reflectivity of over 99.99% is employed to divide the laser into two segments. The low-power laser that passes through is directed towards the laser quality monitor (LQM), while the high-power reflected laser is collected by a power meter (PM). To monitor the spectra and timing characteristics of the laser, an optical spectrum analyzer (OSA) and a photodetector (PD) are used.

3.3. Output characteristics

We fixed the seed laser at 100 W and measured the output spectra under various output DF lengths, as shown in

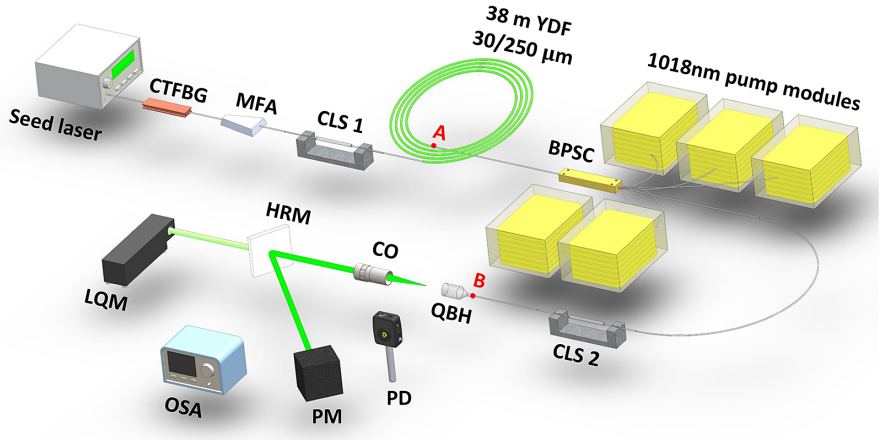

Figure 5. Experimental setup of the 10 kW counter tandem-pumped amplifier.

https://doi.org/10.1017/hpl.2024.21 Published online by Cambridge University Press

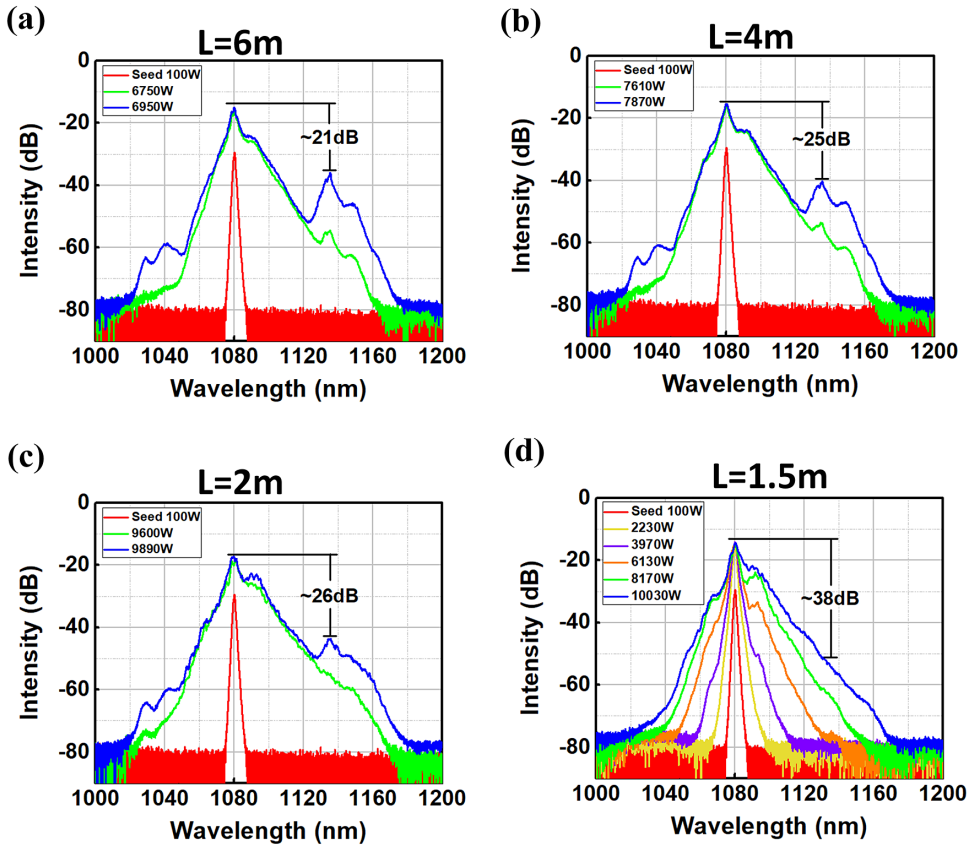

Figure 6. Laser output spectra with output DF length (point A to point B in Figure 5) of (a) $L = 6$ m, (b) $L = 4$ m, (c) $L = 2$ m and (d) $L = 1.5$ m.

Figure 6. It is found in Figures 6(a)–6(c) that the Raman Stokes laser at approximately 1135 nm emerges and grows dramatically as power increases near the SRS threshold. The maximum measured Raman-to-signal ratios for the 6, 4 and 2 m DF cases were –21 dB at 6950 W, –25 dB at 7870 W and –26 dB at 9890 W, respectively. In addition, across all three spectra, a nonlinear increase in Raman light intensity was observed prior to reaching the peak power. Therefore, it was not rigorous but reasonable to roughly consider 6950, 7870 and 9890 W as the corresponding SRS threshold powers. In this manner, as the DF length decreased from 6 to 4 m and 4 to 2 m, the SRS threshold increased by 920 and 2020 W, respectively. These results indicated that the shorter the DF length, the greater the enhancement of the SRS threshold by reducing the DF per unit length. Finally, we optimized the DF length to 1.5 m and obtained an over 10 kW fiber laser, the spectrum of which is shown in Figure 6(d). The 3 dB spectral linewidth increases from approximately 1.36 nm of the seed laser (100 W) to approximately 3.72 nm at 10,030 W. Due to four-wave mixing between modes[38,39], sub-peaks are generated near 1070 and 1090 nm. The strength of these sub-peaks increases rapidly as the power increases, resulting in a rapid broadening in the 10 dB spectral linewidth. The 10 dB spectral linewidth is 18.56 nm at 10,030 W. Although the 60 dB spectral linewidth has been broadened to over 1160 nm at the highest power, there is no clearly identifiable Raman characteristic peak near 1135 nm. The Raman-to-signal ratio is about –38 dB at the maximum power, demonstrating the excellent SRS suppression of the system.

Figure 7(a) shows the output power and corresponding optical-to-optical (O-O) efficiency under different pump powers. The output power increases almost linearly with the pump power and the maximum output power reaches 10,030 W at an injected pump power of 12,470 W, corresponding to an O-O efficiency of 79.6%. The power fluctuation (see Figure 7(b)) at full power during the test is approximately 0.7 %, which indicates a reliable stability of the fiber laser. Figure 7(c) shows the time trace and corresponding Fourier transform at 10,030 W. The time trace is stable and no characteristic peak could be observed in the frequency domain, indicating that no MI occurred at the maximum power.

Figure 8(a) shows the evolution of beam quality under different output powers. The captured profiles at the beam waist maintain good circularity without obvious distortion. While scaling the power from 1000 to 8000 W, the beam quality M^2 slightly varies within the range of 1.65–1.75. As the output laser power exceeds 8 kW, the beam quality slowly deteriorates with the increase of power. Specifically, the M^2 value is 1.85 at 9200 W and increases to 1.92 at 10,030 W

https://doi.org/10.1017/hpl.2024.21 Published online by Cambridge University Press

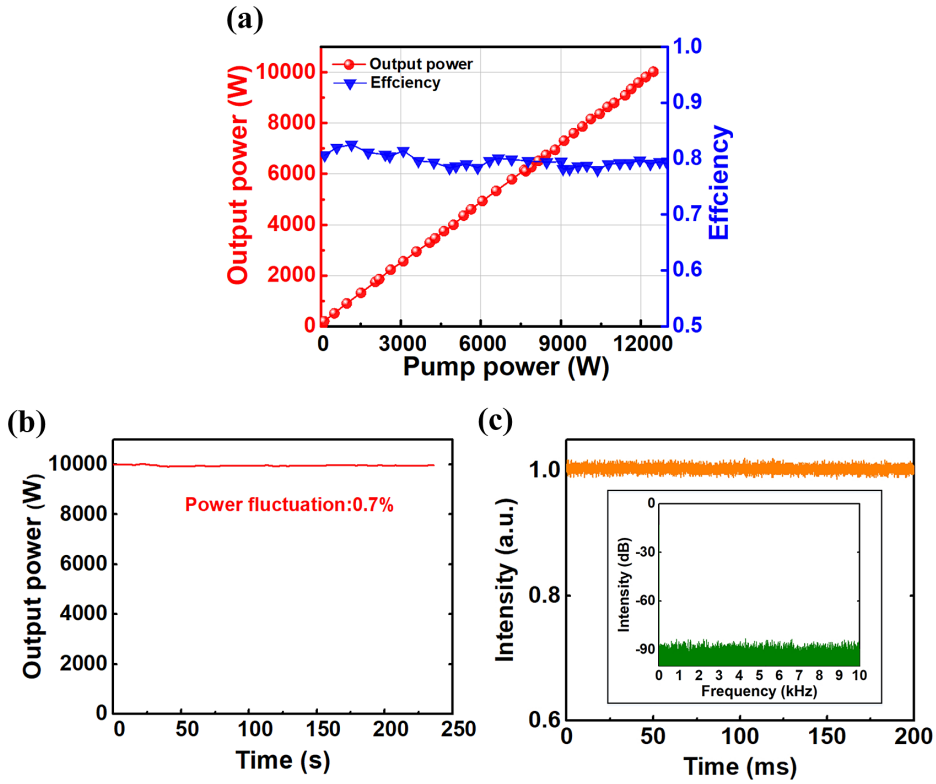

Figure 7. (a) Output power and corresponding optical-to-optical efficiency under different pump powers. (b) Power fluctuations at 10,030 W. (c) Time trace and corresponding Fourier transform under the operation power of 10,030 W.

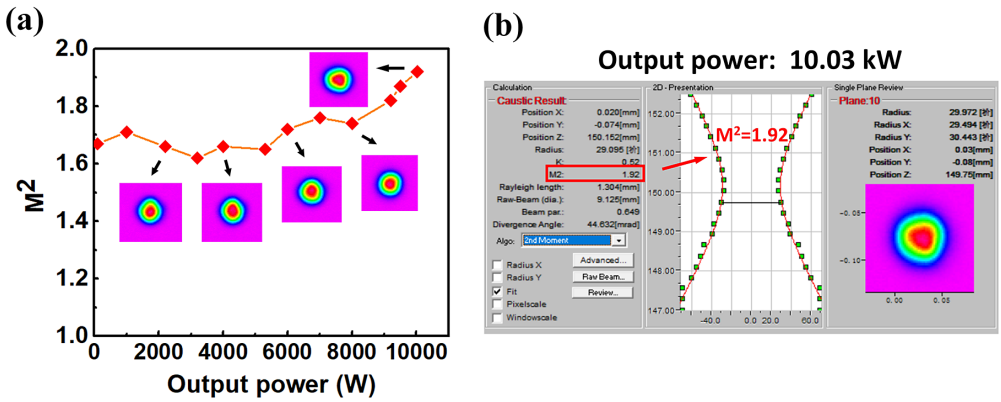

Figure 8. (a) Beam quality M^2 and beam profiles at the waist (insert) under different output powers. (b) Screenshot of the beam quality measurement software at the operation power of 10,030 W.

(refer to Figure 8(b)). The degradation of beam quality at high power could potentially be attributed to the thermal effects of the BPSC, CO, and HRM.

Although many research groups have achieved more than 10 kW monolithic fiber lasers, their beam qualities are far from single mode[23,24,40,41]. Our work achieved an M^2 of 1.92, representing the highest beam quality achieved in over 10 kW YDFLs based on conventional double-clad Yb-doped fiber. We have not yet observed any physical limits, such as SRS, MI or thermal damage. Further power scaling is limited by the available pump powers.

4. Conclusion

To sum up, we have systematically studied the impact of fiber length on the SRS threshold in the tandem pumping system and uncovered a distinct feature of counter-pumping, which differs from co-pumping. For the co-pumping scheme, it is useful to improve the SRS threshold by decreasing the length of either the YDF or DF. For the counter-pumping scheme, reducing the DF length was much more effective in mitigating SRS than reducing the YDF. By decreasing the DF length from 6 to 1.5 m, we increased the SRS

https://doi.org/10.1017/hpl.2024.21 Published online by Cambridge University Press

threshold from 6950 to 10,030 W in a counter tandem-pumped amplifier. At the maximum power of 10,030 W, the signal power was 38 dB higher than the Raman light power, and the beam quality factor M^2 was 1.92. Further power scaling was constrained by the available pump power. We hope this work will help deepen the understanding of SRS effects, and offer guidance for optimizing fiber in the high-power fiber laser community.

Acknowledgements

This work was supported by the National Key Research and Development Program of China (No. 2022YFB3606000) and the National Natural Science Foundation of China (Nos. 62035015 and 62305390). The authors wish to thank Liang Xiao, Chongwei Wang and Mengfan Cui for their helpful assistance in the experiment.

References

1. C. Wirth, O. Schmidt, A. Kliner, T. Schreiber, R. Eberhardt, and A. Tünnermann, Opt. Lett. **36**, 3061 (2011).
2. P. Zhou, H. Xiao, J. Leng, J. Xu, Z. Chen, H. Zhang, and Z. Liu, J. Opt. Soc. Am. B **34**, A29 (2017).
3. P. Yan, Z. Wang, X. Wang, Q. Xiao, Y. Huang, J. Tian, D. Li, and M. Gong, IEEE Photonics J. **11**, 1501612 (2019).
4. C. A. Codemard, J. K. Sahu, and J. Nilsson, IEEE J. Quantum Electron. **46**, 1860 (2010).
5. H. Wu, R. Li, H. Xiao, L. Huang, P. Ma, T. Yao, J. Xu, J. Leng, Z. Pan, and P. Zhou, Proc. SPIE **12595**, 125952D (2023).
6. Q. Chu, Q. Shu, Z. Chen, F. Li, D. Yan, C. Guo, H. Lin, J. Wang, F. Jing, C. Tang, and R. Tao, Photonics Res. **8**, 595 (2020).
7. C. Zhang, R. Tao, M. Li, X. Feng, R. Liao, Q. Chu, L. Xie, H. Li, B. Shen, L. Xu, and J. Wang, J. Lightwave Technol. **41**, 671 (2022).
8. C. Zhang, L. Xie, H. Li, B. Shen, X. Feng, M. Li, R. Tao, and J. Wang, IEEE Photonics J. **14**, 3016605 (2022).
9. V. Distler, F. Möller, M. Strecker, G. Palma-Vega, T. Walbaum, and T. Schreiber, Opt. Express **28**, 22819 (2020).
10. V. Distler, F. Möller, B. Yildiz, M. Plötner, C. Jauregui, T. Walbaum, and T. Schreiber, Opt. Express **29**, 16175 (2021).
11. K. Hejaz, M. Shayganmanesh, R. Rezaei-Nasirabad, A. Roohforouz, S. Azizi, A. Abedinajafi, and V. Vatani, Opt. Lett. **42**, 5274 (2017).
12. H. Zhang, H. Xiao, X. Wang, P. Zhou, and X. Xu, Opt. Lett. **45**, 3394 (2020).
13. C. Jauregui, C. Stihler, and J. Limpert, Adv. Opt. Photonics **12**, 429 (2020).
14. T. Schreiber, A. Liem, E. Freier, C. Matzdorf, and A. Tünnermann, Proc. SPIE **8961**, 89611T (2014).
15. F. Kong, C. Dunn, J. Parsons, M. T. Kalichevsky-Dong, T. W. Hawkins, M. Jones, and L. Dong, Opt. Express **24**, 10295 (2016).
16. W. Liu, P. Ma, H. Lv, J. Xu, P. Zhou, and Z. Jiang, Opt. Express **24**, 26715 (2016).
17. V. Bock, A. Liem, T. Schreiber, R. Eberhardt, and A. Tünnermann, Proc. SPIE **10512**, 105121F (2018).
18. T. Li, W. Ke, Y. Ma, Y. Sun, and Q. Gao, J. Opt. Soc. Am. B **36**, 1457 (2019).
19. Z. Wang, W. Yu, J. Tian, T. Qi, D. Li, Q. Xiao, P. Yan, and M. Gong, IEEE J. Quantum Electron. **57**, 6800109 (2021).
20. W. Liu, S. Ren, P. Ma, and P. Zhou, Chin. Phys. B **32**, 034202 (2023).
21. J. Dai, C. Shen, N. Liu, L. Zhang, H. Li, H. He, F. Li, Y. Li, J. Lv, L. Jiang, Y. Li, H. Lin, J. Wang, F. Jing, and C. Gao, Opt. Fiber Technol. **67**, 102738 (2021).
22. L. Zhang, F. Lou, and M. Wang, Chin. J. Lasers **48**, 1315001 (2021).
23. T. Qi, D. Li, G. Fu, Y. Yang, G. Li, L. Wang, S. Du, P. Yan, M. Gong, and Q. Xiao, Opt. Lett. **48**, 1794 (2023).
24. S. Du, T. Qi, D. Li, P. Yan, M. Gong, and Q. Xiao, IEEE Photonics Technol. Lett. **34**, 721 (2022).
25. J. Kim, P. Dupriez, C. Codemard, J. Nilsson, and J. K. Sahu, Opt. Express **14**, 5103 (2006).
26. L. A. Zenteno, J. Wang, D. T. Walton, B. A. Ruffin, M. J. Li, S. Gray, A. Crowley, and X. Chen, Opt. Express **13**, 8921 (2005).
27. J. M. Fini, M. D. Mermelstein, M. F. Yan, R. T. Bise, A. D. Yablon, P. W. Wisk, and M. J. Andrejco, Opt. Lett. **31**, 2550 (2006).
28. H. Wu, R. Li, H. Xiao, L. Huang, H. Yang, Z. Pan, J. Leng, and P. Zhou, Opt. Express **29**, 31337 (2021).
29. C. Wang, H. Xiao, X. Xi, W. Liu, R. Li, Z. Pan, H. Yang, Z. Yan, Z. Chen, L. Huang, M. Wang, B. Yang, X. Wang, P. Ma, and Z. Wang, Opt. Express **31**, 40980 (2023).
30. X. Chen, T. Yao, L. Huang, Y. An, H. Wu, Z. Pan, and P. Zhou, Adv. Fiber Mater. **5**, 59 (2023).
31. C. Shi, R. T. Su, H. W. Zhang, B. L. Yang, X. L. Wang, P. Zhou, X. J. Xu, and Q. S. Lu, IEEE Photonics J. **9**, 1502910 (2017).
32. G. Wang, J. Song, Y. Chen, S. Ren, P. Ma, W. Liu, T. Yao, and P. Zhou, High Power Laser Sci. Eng. **10**, e22 (2022).
33. I. Hagop and D. G. Gregory, *High Power Laser Handbook* (McGraw-Hill Education, New York, 2011).
34. R. Li, H. Li, H. Wu, H. Xiao, J. Leng, L. Huang, Z. Pan, and P. Zhou, Opt. Express **31**, 24423 (2023).
35. Y. Wang, Opt. Eng. **44**, 114202 (2005).
36. G. P. Agrawal, J. Opt. Soc. Am. B **28**, A1 (2011).
37. P. Ma, H. Xiao, W. Liu, H. Zhang, X. Wang, J. Leng, and P. Zhou, High Power Laser Sci. Eng. **9**, e45 (2021).
38. N. Vukovic, J. S. Chan, C. A. Codemard, and M. N. Zervas, in *Optica Advanced Photonics Congress 2022* (Optica Publishing Group, 2022), paper SoW2I.3.
39. L. Yin, Z. Han, and R. Shu, Opt. Express **31**, 10840 (2023).
40. H. Lin, L. Xu, C. Li, Q. Shu, Q. Chu, L. Xie, C. Guo, P. Zhao, Z. Li, J. Wang, F. Jing, and X. Tang, Results Phys. **14**, 102479 (2019).
41. J. Shi, J. Wu, H. Hu, T. Du, and D. Yan, Proc. SPIE **12169**, 121695J (2022).

https://doi.org/10.1017/hpl.2024.21 Published online by Cambridge University Press